

High-speed, FPGA-based photon-counting fluorometer with high data-gathering efficiency

Tetsuo Iwata and Takahiko Mizuno

Graduate School of Science and Technology, Tokushima University, 2-1
Minami-Jyosanjima, Tokushima 770-8506, Japan

E-mail: iwata@tokushima-u.ac.jp

Abstract. We have developed a low-cost, high-efficiency fluorometer using a field-programmable gate array and simultaneous detection of photoelectron pulse trains. The fluorometer covers a time span of 64 ns with a resolution of 1.0 ns/channel. Depending on the number of channels, the signal-gathering efficiency was improved by a factor of 100 relative to that of conventional time-correlated single-photon-counting. This is assuming that the fluorescence intensity is moderately high but still requires photon counting. The dead time for building a histogram has been reduced to zero, which means that the upper limit of the repetitive excitation frequency could exceed that determined by the time span. We describe instrumental details and demonstrate the basic performance.

Keywords: fluorescence lifetime, photon counting, FPGA, instrumentation, spectroscopic technique.

1. Introduction

One of the most popular methods for measuring fluorescence lifetimes is time-correlated single-photon counting (TC-SPC) [1-4], which is based on statistical sampling using a time-to-amplitude converter (TAC) as a time analyzer. Although the TAC easily enables time resolution of a few picoseconds, it has two major problems. The first is that it has a low fluorescence signal-gathering efficiency. Therefore, depending on the fluorescence lifetime, the fluorescence intensity incident on a photo-detector has to be severely restricted so that only one photoelectron pulse arrives on average for 100 excitations. Otherwise, the fluorescence decay histogram will be distorted because of the nonlinear count rate of the arrival photons. Hence, the fluorescence intensity must be attenuated, even for samples having high quantum yields. This can be tolerated for samples with extremely low fluorescence intensities, but not for many other samples. The second problem is that the data gathering (or histogram building) efficiency is low because the excitation frequency usually cannot be increased. In TC-SPC, the output voltage from the TAC is processed *via* an analogue-to-digital converter (ADC) and the content of the memory address that corresponds to the ADC value is increased by one. This “add-one” process is repeated continuously to build the fluorescence decay histogram in a multichannel analyzer (MCA) operating in pulse-height-analyzer mode. The time required for one cycle of this process is a dead time that limits the maximum excitation frequency. This problem has been relaxed somewhat with high-count-rate TAC systems, but not solved completely. These two problems result in long measurement times. Thus there have been efforts, especially for biological and medical applications, to shorten measurement times, even at the

cost of time resolution.

The use of multiple TACs operated in parallel has increased the signal-gathering efficiency in proportion to the number of TACs¹. However, critical adjustments of individual TACs are still required, and the data-gathering efficiency is the same as that of a single TAC system. Another way to increase the signal-gathering efficiency is to employ a photoelectron-pulse-train simultaneous-detection method (PPT-SDM), where the fluorescence-induced photoelectron pulse train following pulsed excitation is captured simultaneously. For that purpose, shift-register (SR)-based [5, 6] and vernier chronotron-based methods [7] have been proposed. The former is a commercially available multichannel scaler [8]. Common to both two methods is that the time-series information for photoelectron pulse arrival times is recorded as spatial information in a bit pattern on the SR, or flip-flops, to build the histogram. The signal-gathering efficiency is thus improved markedly, at the cost of time resolution, relative to that of conventional TC-SPC, depending on the number of channels (or measurement time span). However, the data-gathering efficiency decreases with increasing time span. Even if a hardware-based direct-memory-access (DMA) is used for building the histogram, the system dead time cannot be shortened appreciably. [7] For example, if there are total of 50 channels with a time resolution of 1 ns/channel, and the add-one cycle per channel is 1 μ s, then, it takes more than 50 μ s to finish the whole process, resulting in a 20-kHz maximum excitation frequency. Similarly, for a time span of 50 ns, the excitation frequency should be 20 MHz. For the multichannel scaler mentioned above, this can be performed with a multichannel parallel adder (add-one) circuit, resulting in no system dead time. However, this approach is expensive and is not flexible because the hardware specifications are fixed. Other approaches also have been reported, such as use of a digital frequency-domain hardware [9], a high speed time-to-digital converter (TDS) [10], a combination of multiple detectors and TDS [11,12], and a combination of multiple detectors and a multiplexed counting with a single TAC [13]. Although those approaches seem promising in many applications, they are somewhat complicated or cost consuming to build up.

Here, we demonstrate a PPT-SDM-based fluorometer that uses a field-programmable gate array (FPGA). The array is a highly integrated, rewritable logic device that features: (i) a highly flexible circuit design, (ii) high-speed operation, and (iii) relatively low cost. Many scientific instruments using FPGAs have been reported [14-19]. The time span of the fluorometer is 64.0 ns (64 channels), with a resolution of 1.0 ns and zero dead time for building histogram. Therefore, the maximum excitation frequency is limited only by the time span. Furthermore, a laboratory-made amplifier/discriminator pair has a 1.5-ns pulse-pair resolution, which improves the signal-gathering efficiency. To achieve a 1.0-ns/channel time resolution, a decoder circuit is incorporated for detecting leading edges of arriving photoelectron pulses.

2. Instrumental

2.1. Principle of operation

Figure 1 depicts the working principle of the PPT-SDM. As shown in Figure 1(a), when the fluorescence intensity is low, the probability distribution of generating fluorescence photons after pulsed excitation is proportional to the amplitude of the observable, high-intensity fluorescence decay (dotted line). In this illustration, two fluorescence photons are depicted. Figure 1(b) shows conventional TAC operation that registers only the first photon when building a histogram; the second photon is not used. This distorts the histogram. To eliminate the distortion, the fluorescence intensity must be attenuated so that only one photon is detected per excitation. Usually, the number of photons counted per excitation is restricted to 0.01, resulting in a low signal-detection efficiency. In contrast, as

¹ For example, a multichannel-TAC NAES-500/550 system had been manufactured by HORIBA Ltd. (Kyoto, Japan) from 1982 to 2000.

shown in Figure 1(c), multiple fluorescence photons generated after pulsed excitation can be fed into the SR driven by a high-frequency shift clock of the PPT-SDM system, and then recorded as a spatial bit pattern. The first problem of the conventional TAC system is therefore solved. In a conventional PPT-SDM system, however, the bit pattern information recorded on the SR is read by a slow shift clock, and then the add-one procedure is performed to build the histogram. The content of a random-access-memory corresponding to each channel (bit) of the SR is increased by one. The time required for this process increases with the number of channels, even if the DMA is employed, resulting in a long dead time. Thus, a large reduction in measurement time cannot always be attained. To solve the second problem, we developed a system shown in Figure 1(d), where the bit pattern information on the SR is simultaneously fed into counter arrays *via* latches. The number of the counter is the same as that of the channel, and the counter arrays work as a memory bank for building and storing the histogram. Because the timing of the latch is synchronized with the excitation, the system dead time for building the histogram is zero.

In the PPT-SDM system, the resolution time is determined by the shift-clock frequency that drives the SR, which can be up to 500-MHz. To further improve the time resolution, we arranged two SRs [Figure 2(a)] that were operated by shift clocks with mutually inverted phases. Therefore, the clock frequency is essentially 1.0 GHz, with 1.0-ns time resolution. Furthermore, as shown in Figure 2(b), a decoder circuit was inserted between the SRs and the counter arrays so that the leading edge of each photoelectron pulse could be extracted, thereby ensuring the overall 1.0-ns time resolution (but not for a single excitation cycle). The signal-gathering efficiency of the PPT-SDM is limited by the 1.5-ns pulse-pair resolution of the pulse amplifier/discriminator pairs connected to the photomultiplier tube (PMT).

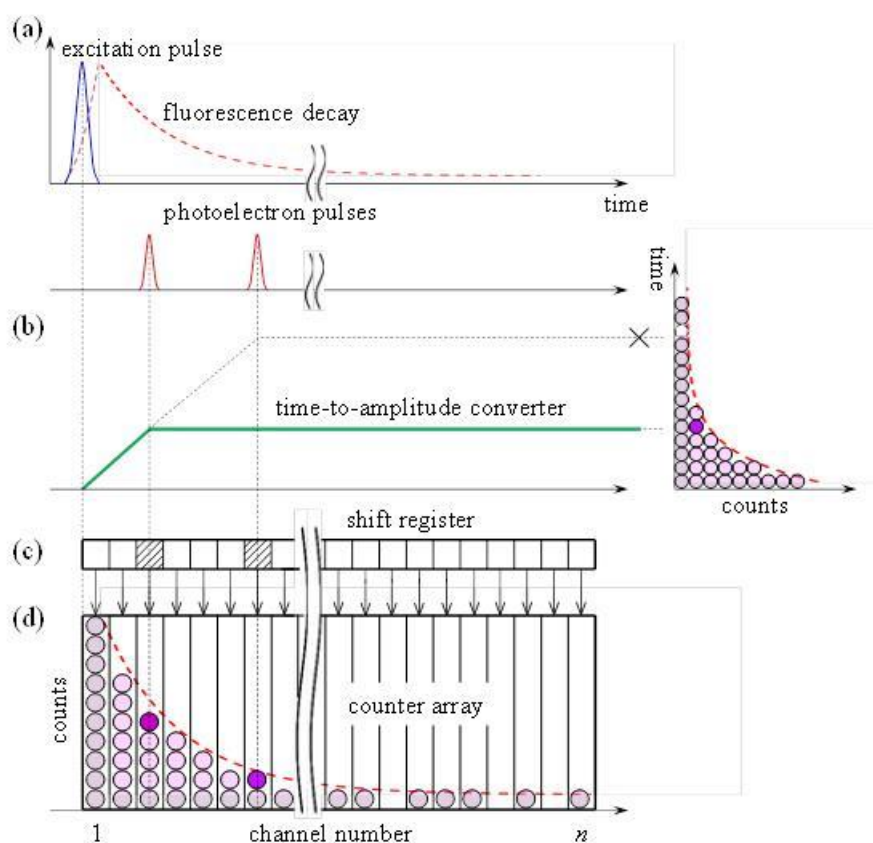


Figure 1. (a) Photoelectron pulse trains after pulsed excitation. A dotted line shows the fluorescence decay — that is observable when its intensity is high. (b) Operation of a conventional TAC system.

(c) Working principle of the PPT-SDM. (d) A PPT-SDM-based system combined with counter arrays.

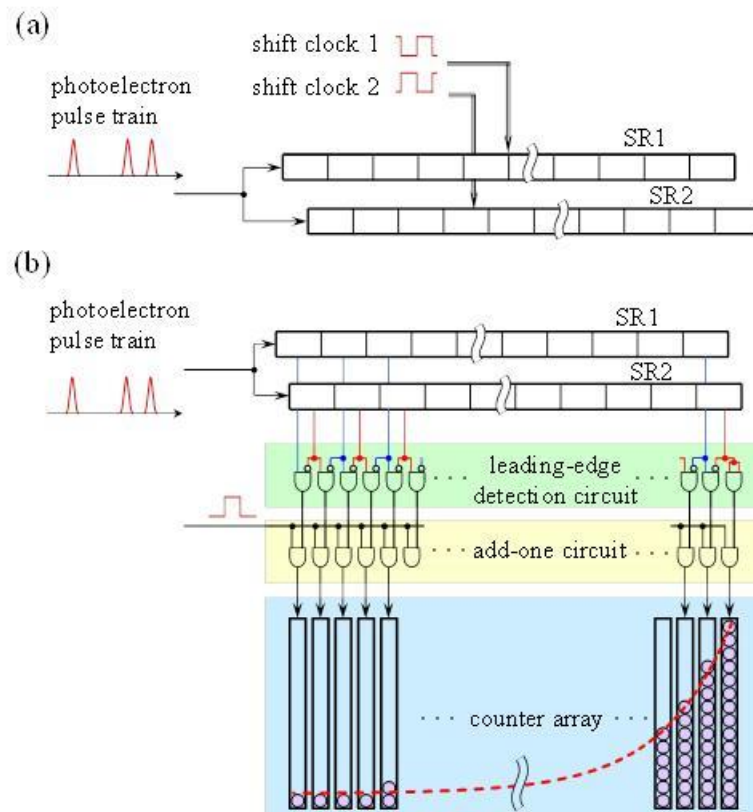


Figure 2. (a) Two series of SRs that are driven by shift clocks with mutually inverted phases. (b) An AND-gate decoder for detecting leading edges of a photoelectron pulse train.

2.2. PPT-SDM-based fluorometer

Figure 3 is a schematic of the PPT-SDM-based fluorometer. The excitation source was a commercially available 375-nm, 60-ps picosecond light pulser (PLP-10-038, Hamamatsu Photonics K. K., Shizuoka, Japan) operated at 10 or 20 MHz. Fluorescence was focused onto a PMT (H6780-01, Hamamatsu Photonics K. K.) after passing through a long-wavelength-pass filter (LPF). Photoelectron pulses from the PMT were connected to the FPGA system *via* a laboratory-made amplifier/discriminator pair described below.

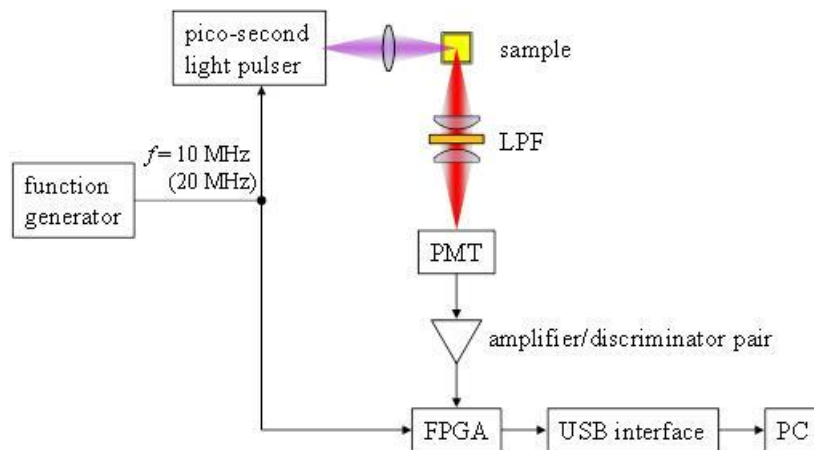


Figure 3. Schematic of the PPT-SDM-based fluorometer.

2.3. Photon-counting unit in the FPGA

Figure 4 is a schematic of the photon-counting unit for the PPT-SDM-based fluorometer that was constructed on an FPGA board (Cyclone V GX Starter Kit, Terasic Inc., Hsinchu, Taiwan). The 10- or 20-MHz repetition frequency of the excitation pulse was set by a phase-locked-loop (PLL) circuit so that $mf=500$ MHz ($m=50$ or 25), where f stands for an excitation frequency and m is an integer. The fluorescence-induced PMT photoelectron pulse train is fed into a series of two 32-bit SRs driven by the 500-MHz shift clock and recorded as a spatial bit pattern. As described above, the SR shift clocks are mutually out of phase, producing 1.0-ns time resolution essentially. To build the fluorescence decay histogram, the 2×32 -bit pattern information is added and recorded on 64-channel, 32-bit-counter arrays in parallel during completion of the whole shift after every excitation cycle. Thus, the dead time for histogram building is zero when f is larger than that determined by the time span (here, it is 64 ns or 15.625 MHz). The histogram data is read out and sent to a personal computer (PC) through a USB interface every 0.1 sec, asynchronous with the excitation. The leading-edge detection circuit described in Figure 2(b) ensures overall 1.0-ns time resolution.

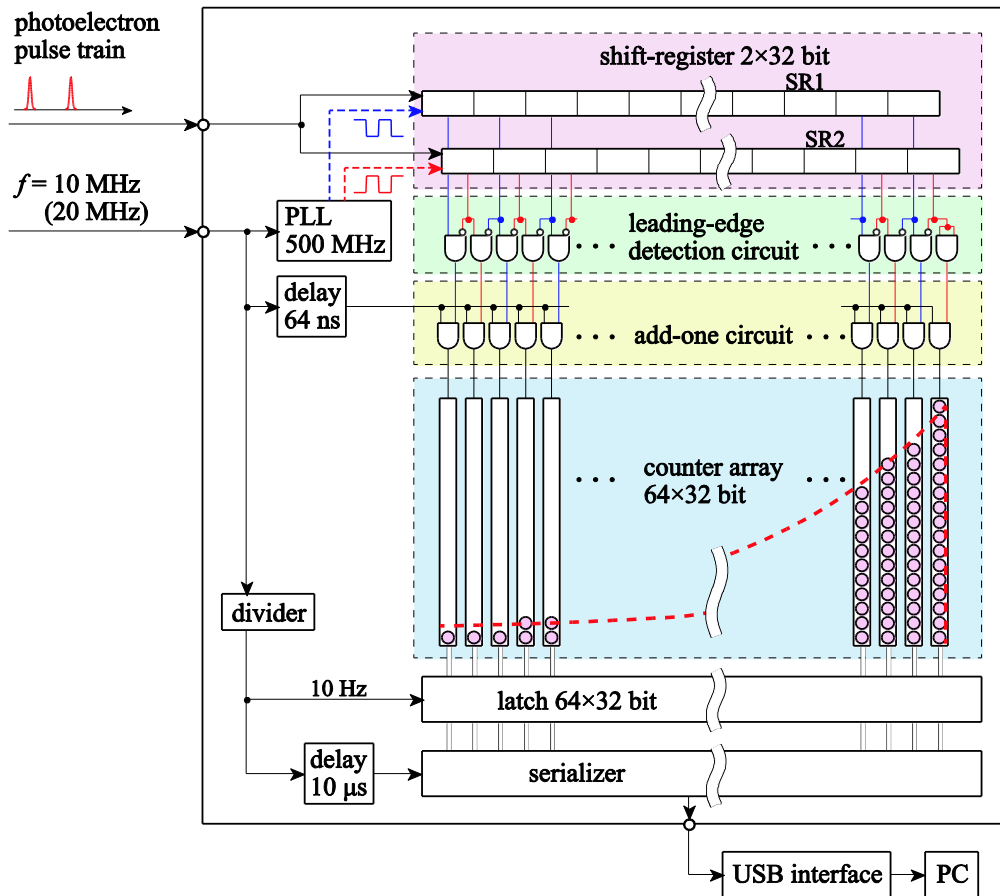


Figure 4. Schematic of PPT-SDM-based photon counter constructed on an FPGA board.

2.4. Pulse amplifier/discriminator pair

Figure 5 is a circuit diagram of a laboratory-made pulse amplifier/discriminator pair that uses a high-speed monolithic amplifier and comparator. PMT photoelectron pulses are inputted into the amplifier (GN1021, DC~1.5 GHz frequency bandwidth, 25-dB gain, Panasonic Co., Osaka, Japan) and then **inputted** into the comparator (ADCMP604BKSZ, 600-ps output rise time and fall time, 70-ps propagation delay time, Analog Devices, MA, USA). The pulse-pair resolution is 1.5 ns. The output pulse from the pair is **inputted** into the FPGA board at a LVDS (low voltage differential signaling) level. The frequency bandwidth of the PMT is around 1.0 GHz. Therefore, the dominant dead time in the signal-gathering efficiency in the system is still determined by the pulse pair resolution of the pulse amplifier/discriminator pair. Another problem caused by the PMT is timing jitter mainly introduced by the fluctuation of electron transit time of PMT, around 100 ps depending on the applied voltage, which restricts precision in fluorescence lifetime measurements.

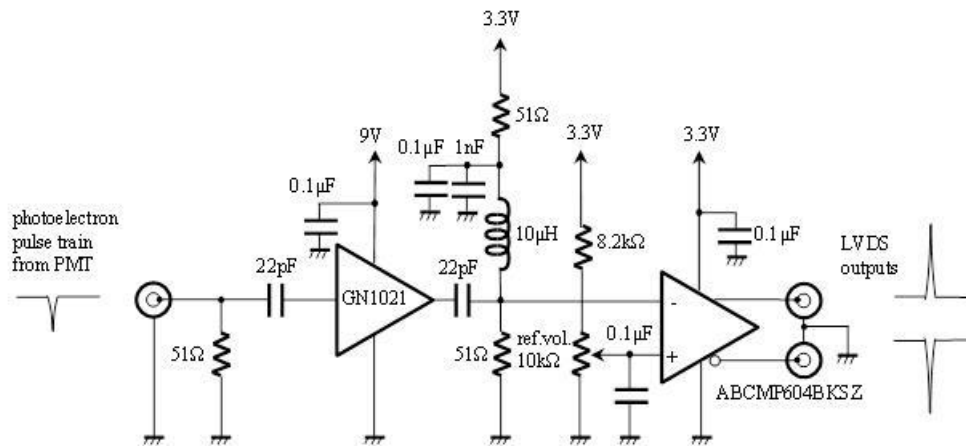


Figure 5. Circuitry diagram of high-speed pulse amplifier/discriminator pair.

3. Fundamental Performance Tests

3.1. Linearity of the count rate

Figure 6 is a plot of count rate vs. incident light intensity for the PPT-SDM-based fluorometer. The incident light was a dc-driven blue LED (NSPB300B, Nichia Co., Tokushima, Japan) that was attenuated with neutral density filters. The frequency of the trigger signal for the system was fixed at 10 MHz, and the count rate was defined as the average number of photoelectron pulses per one trigger pulse recorded on the 64-bit SR over 64 ns. The linearity of the count rate was degraded at high incident light intensities because of the pulse-pair resolution of the amplifier/discriminator pair. If we define the upper limit of the count rate linearity as a point with a 5.0% deviation from linearity, the value becomes 2.1 at 0.33-nW incident light power. This count rate is about 200 times better than that of conventional TC-SPC [1,13], depending on the number of channels. At the 5.0% point, the number of counts per 0.1 sec was 2.14×10^7 .

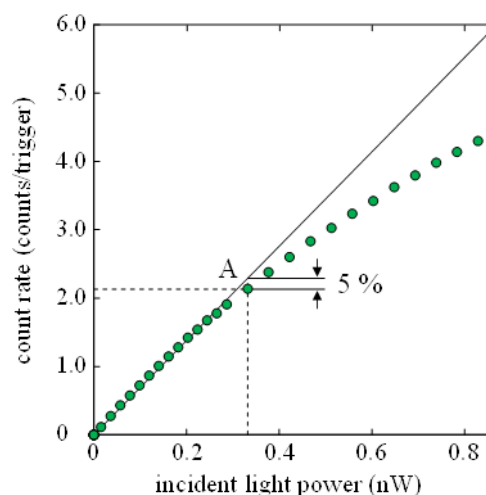


Figure 6. Count rate vs. incident light intensity.

3.2. Differential linearity of the channel width

Figure 7 plots the differential linearity of the channel width (or count uniformity) for each channel. This is a histogram obtained at 0.33-nW light power at point “A” in Figure 6, where the relative standard deviation (RSD) is 0.22%. The value should be 0.17 % theoretically when the incident light obeys Poisson statistics [20]. The deviation might be due to detector noise.

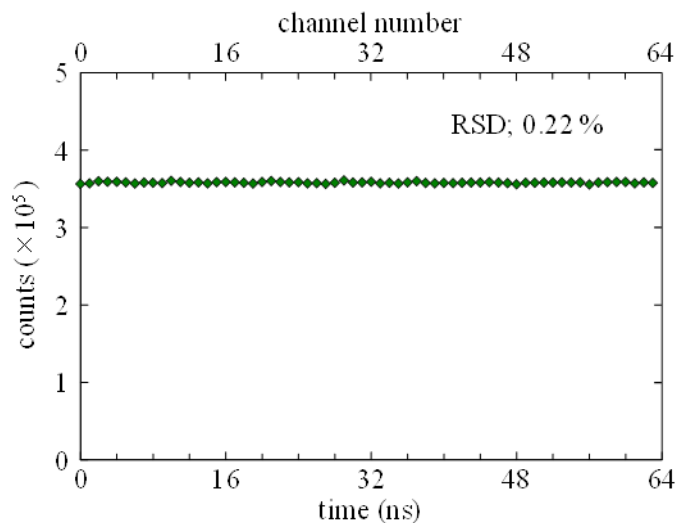


Figure 7. Differential linearity of the channel width. The incident light power was 0.33 nW at point “A” in Figure 6.

3.3. Linearity of the channel interval

Figure 8 plots the linearity of the channel interval, using a digital delay pulse generator (DG645, Stanford Research Systems, Inc., CA, USA). Two pulses whose interval was a maximum of 64 ns were inputted into the FPGA with a 1.0-ns step. The linearity indicates that the time analysis was performed correctly.

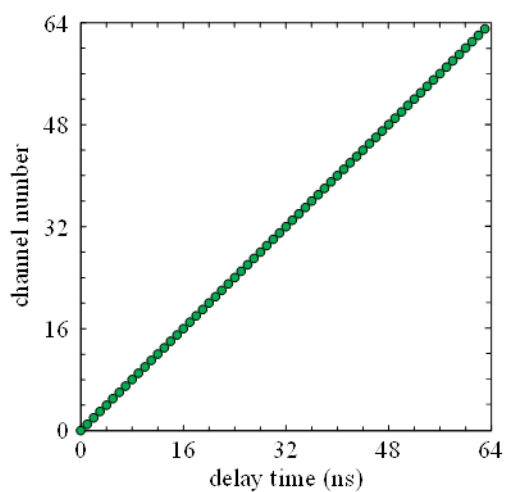


Figure 8. Linearity of the channel interval.

4. Results and discussion

4.1. Fluorescence measurements of standard samples

The performance of the PPT-SDM-based fluorometer was tested with standard fluorescent samples (Figure 9): (a) 10-ppm quinine sulfate in 0.1-N H₂SO₄, (b) 1.0- μ M rhodamine 6G in ethanol, and (c) 1.0- μ M coumarin 152 in ethanol. The excitation wavelength was 375 nm with a repetition frequency of 10 MHz for (a) and 20 MHz for (b) and (c), and an average power of 50 pW. The emission was filtered with an LPF with a -3 dB cutoff wavelength of 420 nm (SCF-50S-42L, SigmaKoki Co., Ltd., Saitama, Japan) for all three samples. The solid lines in Figure 9 are numerically fitted curves assuming that each decay was a single exponential. Dotted lines indicate the pulsed-excitation waveforms. The estimated fluorescence lifetimes τ were derived by convoluting the excitation waveform with the exponential decay by a template matching procedure: (a) 18.4 ns, (b) 4.0 ns, and (c) 1.6 ns, which agreed with the respective literature values [21-23]. The reduced χ -squared values, χ_R^2 , representing the goodness of fit were (a) 1.10, (b) 1.01, and (c) 1.02, respectively. The values of around 1.0 indicate the good fit [1,2]. The measurement times were all 1.0 sec, with count rates of (a) 1.01, (b) 0.22, and (c) 0.15, which demonstrate the superiority of the PPT-SDM relative to conventional TC-SPC. The count rate was defined here as the average number of photoelectron pulses per one excitation. The incident power calculated from the count rates was almost agreed with that measured. For Figure 9(b,c), the repetition frequency was 20 MHz ($m = 50$). Therefore, two decays with an interval of 50 ns were built within the time span of 64 ns, which demonstrate no system dead time for building histogram.

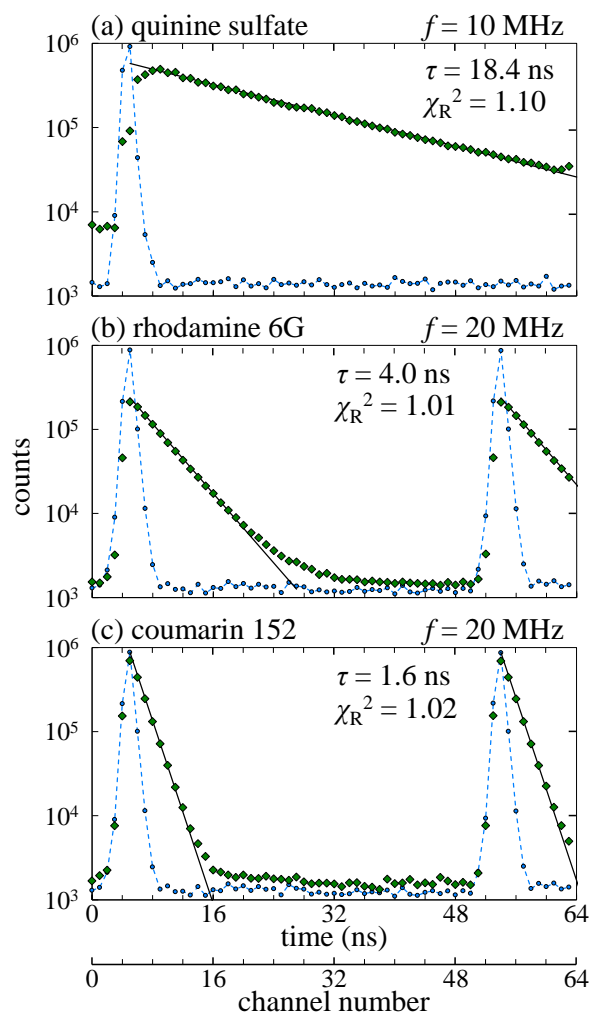


Figure 9. Fluorescence decays for standard samples: (a) 10-ppm quinine sulfate in 0.1-N H_2SO_4 , (b) 1.0- μM rhodamine 6G in ethanol, and (c) 1.0- μM coumarin 152 in ethanol. The dotted lines are pulsed-excitation waveforms. The estimated fluorescence lifetimes τ were (a) 18.4 ns, (b) 4.0 ns, and (c) 1.6 ns.

4.2. Measurements of successive fluorescence decays

To demonstrate the rapid measurement of fluorescence decays with the PPT-SDM-based fluorometer, we carried out successive decay measurements: the series of fluorescence decay measurements with different time elapsed from the origin. The sample was a 2.0 ml solution of 10-ppm quinine sulfate in 0.1-N H_2SO_4 with an added 200- μl droplet of 3.0 w/v% H_2O_2 solution at time $t=0$. Figure 10 plots the fluorescence decays, where τ is 18.4 ns at $t=0$ and 9.6 ns at $t=15$ sec. For each decay histogram, the number of counts at the peak position was 10^5 for a measurement time of 0.1 sec. The χ_R^2 -values for the individual fits were between 1.10 and 1.22. The PPT-SDM-based fluorometer enables such measurements rapidly and precisely, which might be useful as a time-resolved fluorescence detector for high-performance liquid chromatography [24, 25].

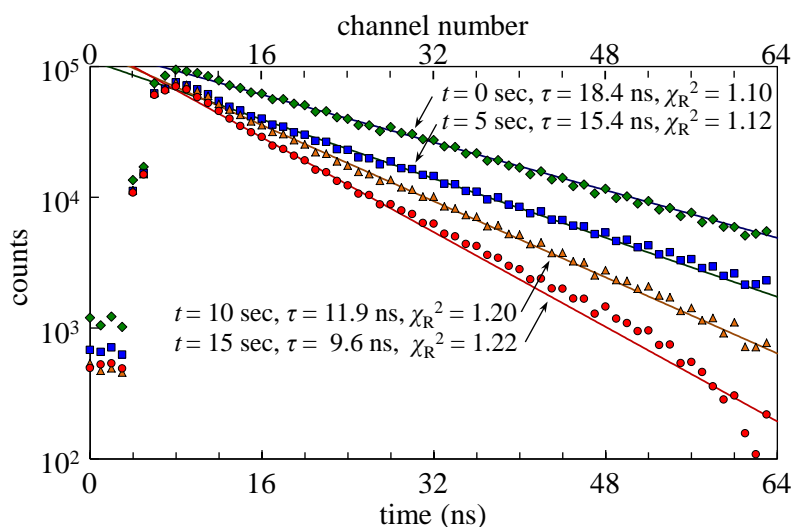


Figure 10. Successive fluorescence decay measurements with different time elapsed from the origin. The sample was a 2.0-ml solution of 10-ppm quinine sulfate in 0.1-N H_2SO_4 , with a 200- μl droplet of 3.0-w/v% H_2O_2 solution added at $t=0$.

5. Conclusions

We constructed a PPT-SDM-based fluorometer with a signal-detection efficiency greater than 200 times that achieved by conventional TC-SPC (depending on the number of channels). A FPGA enabled markedly improved data collection efficiency because of the zero dead time to build a histogram. Thus, measurement times were reduced for samples with moderately high fluorescence intensities. The FPGA also allows the number of channels to be changed with ease. The 1.0-ns/channel time resolution might be further improved by using a SERDES (serializer/deserializer) circuit embedded in a more advanced FPGA chip [26]. A PPT-SDM-based fluorescence-lifetime Hadamard-imaging microscope [27] is a potential application.

Acknowledgement

This work was supported in part by a Grant-in-Aid for Scientific Research B (No. 26289066) from the Japan Society for the Promotion of Science (JSPS).

References

- [1] O'Connor D V and Phillips D 1984 *Time-correlated Single Photon Counting* (New York: Academic)
- [2] Lakowicz J R 2006 *Principles of Fluorescence Spectroscopy 3rd ed.* (New York: Springer).
- [3] Buller G S and Collins R J 2010 Single-photon generation and detection *Meas. Sci. Technol.* **21** 012002
- [4] Hirvonen L M and Suhling K 2017 Wide-field TCSPC: methods and applications *Meas. Sci. Technol.* **28** 012003
- [5] Lawton M, Bolden R C and Shaw M J 1976 A 10-ns multichannel photon counter *J. Phys. E* **9**

686-690

- [6] Kleinfeld T and Ziegler H 1982 A multichannel photon counter with a time resolution of 2.5 ns *J. Phys. E* **15** 888-890
- [7] Iwata T, Uchida T and Minami S 1985 A nanosecond photon-counting fluorimetric system using a modified multichannel vernier chronotron *Appl. Spectrosc.* **39** 101-109
- [8] Becker W 2005 *Advanced Time-Correlated Single Photon Counting Techniques* (Berlin: Springer)
- [9] Colyer R A, Lee C and Gratton E 2008 A Novel fluorescence lifetime imaging system that optimizes photon efficiency *Micros Res Tech* **71** 201-213
- [10] Wahl M, Rahn H-J, Gregor I, Erdmann R and Enderlein J 2007 Dead-time optimized time-correlated photon counting instrument with synchronized, independent timing channels *Rev. Sci. Instrum.* **78** 0331066
- [11] Krstajić N, Levitt J, Poland S, Ameer-Beg S and Henderson R 2015 256×2 SPAD line sensor for time resolved fluorescence spectroscopy *Opt. Express* **23**, 5653-5669, 2015
- [12] Arlt J, Tyndall D, B. R. Rae B R, Li D -U, Richardson J A and Henderson R K 2013 A study of pile-up in integrated time-correlated single photon counting systems *Rev. Sci. Instrum.* **84** 103105
- [13] Suhling K, McLoskey D and Birch D J S 1996 Multiplexed single-photon counting. II. The statistical theory of time-correlated measurements *Rev. Sci. Instrum.* **67** 2238-2246
- [14] Reestelli A, Abbiati R and Geraci A 2005 Digital field gate array-based lock-n amplifier for high-performance photon counting applications *Rev. Sci. Instrum.* **76** 093115
- [15] Buchholz J, Krieger J W, Mocsár G, Kreith B, Charbon E, Vámosi G, Kebschull U and Langowski J 2012 FPGA implementation of a 32x32 autocorrelator array for analysis of fast image series *Opt. Express* **20** 17767-17782
- [16] Cuccato A, Antonioli S, Crotti M, Labanca I, Gulinatti A, Rech I and Ghioni M 2013 Complete and compact 32-channel system for time-correlated single-photon counting measurements *IEEE Photonics J.* **5** 6801514
- [17] Gong S, Labanca I, Rech I and Ghioni M 2014 A 32-channel photon counting module with embedded auto/cross-correlators for real-time parallel fluorescence correlation spectroscopy *Rev. Sci. Instrum.* **85** 103101
- [18] Nishimura G 2015 Note: Design of a full photon-timing recorder down to 1-ns resolution for fluorescence fluctuation measurements *Rev. Sci. Instrum.* **86** 106108
- [19] Antonioli S, Miari L, Cuccato A, Crotti M, Rech I and Ghioni M 2016 8-channel acquisition system for time-correlated single-photon counting *Rev. Sci. Instrum.* **84** 064705
- [20] Holzapfel C 1974 On statistics of time to amplitude converter systems in photon counting devices *Rev. Sci. Instrum.* **45** 894-896
- [21] O'Connor D V, Meech S R and Phillips D 1982 Complex fluorescence decay of quinine bisulphate in aqueous sulphuric acid solution *Chem. Phys. Lett.* **88** 22-26
- [22] Madge D, Wong R and Seybold P G 2002 Fluorescence quantum yields and their relation to lifetimes of rhodamine 6G and fluorescein in nine solvents: Improved absolute standards for quantum yields *Photochem. Photobiol.* **75** 327-334
- [23] Dahiya P, Kumbhakar M, Mukherjee T and Pal H 2005 Effect of protic solvents on twisted intramolecular charge transfer state formation in coumarin-152 and coumarin-481 dyes *Chem. Phys. Lett.* **414** 148-154
- [24] Iwata T, Senda M, Kurosu Y, Tsuji A and Maeda M 1997 Construction of time-resolved fluorescence detector for amino compounds after high-performance liquid chromatography using europium chelate *Anal. Chem.* **69** 1861-1865
- [25] Iwata T, Koshoubu J, Kurosu Y and Araki T 1999 Time-resolved high-performance liquid chromatography using a nanosecond pulsed light source for detecting lanthanide-chelated compounds *J. Chromatogr. A* **859** 13-21
- [26] Altera 2016 Stratix V Device Handbook vol 2 Transceivers
Url: www.altera.com/en_US/pdfs/literature/hb/stratix-v/stx5_xcvr.pdf (Accessed: 27 January 2017)

[27] Mizuno T and Iwata T 2016 Hadamard-transform fluorescence-lifetime imaging *Opt. Express* **24** 8202-8213